

# Digital Continuous-Variable Quantum Key Distribution

Ziyang Chen,<sup>1</sup> Xiangyu Wang,<sup>2</sup> Song Yu,<sup>2</sup> Zhengyu Li,<sup>3,\*</sup> and Hong Guo<sup>1,†</sup>

<sup>1</sup>State Key Laboratory of Advanced Optical Communication Systems and Networks, School of Electronics, and Center for Quantum Information Technology, Peking University, Beijing 100871, China

<sup>2</sup>State Key Laboratory of Information Photonics and Optical Communications, Beijing University of Posts and Telecommunications, Beijing 100876, China

<sup>3</sup>Huawei Technologies Co., Ltd., Shenzhen 518129, China

(Dated: July 2022)

Quantum key distribution (QKD) provides an attractive key-sharing technology for distant users with information-theoretic security. QKD with continuous variables (CV) offers extraordinary superiority by the use of standard telecom components, thereby promoting large-scale metropolitan applications. Modern CVQKD has introduced digital signal processing (DSP) technologies, which paves the way towards ultra-high secret key generation speed with tens of GHz bandwidth, thus we denote it as *digital* CVQKD. However, the security analysis of such a high-bandwidth system with DSP is beyond the traditional analysis method with single-mode description. Herein, we generalize the practical system model with continuous-mode quantum optics, in which data sampling and linear data processing can be described, thus naturally concludes a general method for the security analysis and performance evaluation of linear DSP algorithms. Properly calibrating the shot-noise unit plays a crucial role, once again revealing the essence of vacuum noise to the security of CVQKD.

Quantum key distribution (QKD) [1–3] promises the information-theoretically secure symmetric key distribution for distant partners. The past three decades have witnessed rapid development of QKD technologies, and growth of QKD network deployment over the world, showing various security applications [4–11]. Within the QKD family, continuous-variable (CV) QKD benefits from the use of off-the-shelf commercial telecom components [12, 13], and provides a cost-effective alternative in metropolitan networks. After 20 years since the pioneering GG02 protocol [14] was proposed, the theory [15–20] and experimentation [21–23] of CVQKD have experienced revolutionary progress.

Remarkably, the tremendous breakthroughs of local oscillator (LO) schemes since 2015 [24, 25] have pushed CVQKD to a new stage, in which techniques from modern digital coherent communication were brought in [26–29], thus we noted it as *digital* CVQKD. Especially the digital signal processing (DSP), it significantly improves the signal-to-noise ratio (SNR) by compensating channel drafting and device impairments, which greatly simplifies physical systems. This paves the way towards ultra-high secret key rate with tens of GHz bandwidth CVQKD system, in the meanwhile, this also complicates the security analysis.

There are two barriers for the security analysis of a digital CVQKD system, one is the discrete modulation format and the other is DSP. The former results from the destruction of estimating covariance matrix directly from the measurement results, and recently has been solved with uncertainty principle [30] and semi-defined program [31, 32] methods. While the latter comes from

the difficulty of constructing appropriate measurement operator to describe the output of DSP.

More specifically, current security analysis assumes the receiver conducting quadrature measurements on a single optical mode. DSP algorithms construct a transformation of multiple raw data sampled at different time. To understand what the output represents, time-domain description of system behavior should be introduced, which is beyond traditional single mode description.

In this letter, we develop a generalized practical system model with continuous-mode formalism of optical field operators, and with proper extension, this naturally results in a framework of security analysis for linear DSP algorithms, i.e., pulse shaping, matched filter, frequency conversion, *et. al.* More specifically, in continuous-mode formalism, time-domain field operators can be introduced by Fourier transformation, based on which the sampling process can be well modeled. Linear processing of sampled data can be seen as a recombination of time-domain field operators, which defines a specific *temporal-mode* (TM) field operator [33–35], if normalized by properly calibrated shot-noise unit (SNU). Consequently, the outputs of DSP are actually equivalent to the quadrature measurement results of a specific single TM. Then the rest of security analysis can follow traditional methods.

On another side, the measured state also has certain TM, which is defined by modulation pattern and channel transmission. The mismatch between the measured state's TM and the receiver's TM will lead to an inefficiency of detection. The mission of DSP algorithm is merging this mismatch, thus improves detection efficiency, which coincides with improving SNR in its classical correspondence.

Our work provides a feasible way of analyzing the security and performance of linear DSP algorithms, therefore could be an important guidance for DSP design of digital CVQKD. Linear DSP toolboxes are expected to be

\* E-mail: lizhengyu2@huawei.com

† E-mail: hongguo@pku.edu.cn

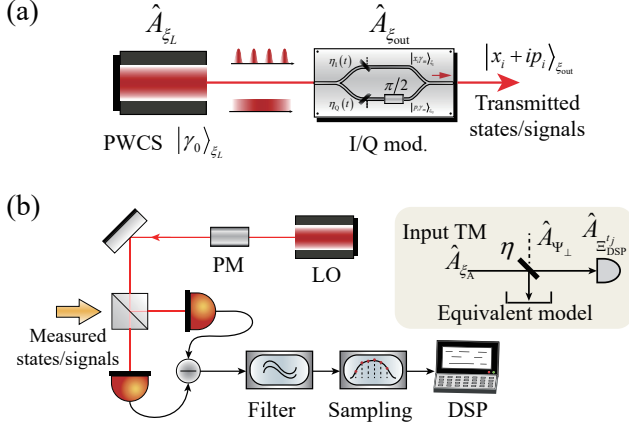


FIG. 1. Models of digital CVQKD. (a) The transmitter prepares a photon-wavepacket coherent state (PWCS) with arbitrary form of envelope  $\xi_L(t)$ ; via the I/Q modulation, the quadratures of the PWCS are modulated by Gaussian distributed random numbers. The carrier can be either a continuous wave or pulsed coherent state. (b) Measured states are fed to a practical receiver, interfering with the local oscillator (LO) at a balanced beam splitter (BS) and detected by a band-limited homodyne detector (HD) (modeled by an ideal HD and a filter), followed by the sampling and digital signal processing (DSP) devices. The mismatch between measured state's temporal mode (TM) and the receiver's TM is equivalent to a BS with transmittivity of  $\eta$ . PM: phase modulator.

directly employed in CVQKD, which illustrates the importance of our work.

*Temporal modes of continuous-mode states.*—We start by introducing the basics of continuous-mode formalism of quantum optics, then describing the state preparation phase. Recall that in traditional CVQKD analysis, coherent state is represented by the creation and annihilation operators in terms of single-mode field, given by  $\hat{a}_i^\dagger, \hat{a}_i$ . While in practical system, high-speed modulation will inevitably introduce non-uniform temporal waveform, therefore, continuous-mode formalism of field operators [33, 35, 36] should be introduced, which is widely used in studying continuous-mode quantum optics. By transforming annihilation and creation operators from their discrete-mode counterparts, continuous-mode field operators are defined as  $\hat{a}_i \rightarrow (\Delta\omega)^{\frac{1}{2}} \hat{a}(\omega)$  and  $\hat{a}_i^\dagger \rightarrow (\Delta\omega)^{\frac{1}{2}} \hat{a}^\dagger(\omega)$ , where  $\Delta\omega$  denotes the mode spacing, which satisfies the commutation relation  $[\hat{a}(\omega), \hat{a}^\dagger(\omega')] = \delta(\omega - \omega')$ . In time-domain, it is useful to define the Fourier transforms of  $\hat{a}(\omega)$ , namely  $\hat{a}(t)$ , given by  $\hat{a}(t) = \frac{1}{\sqrt{2\pi}} \int d\omega \hat{a}(\omega) \exp(-i\omega t)$ . Creation operator  $\hat{a}^\dagger(t)$  follows a similar definition.

Based on this, the photon-wavepacket creation operator  $\hat{A}_{\xi_i}^\dagger$  [33, 37] can be defined as

$$\hat{A}_{\xi_i}^\dagger = \int dt \xi_i(t) \hat{a}^\dagger(t), \quad (1)$$

in which the wavepacket  $\xi_i(t)$  usually reads  $\xi_i^0(t) e^{i\omega t}$ ,

as an envelope  $\xi_i^0(t)$  with a carrier  $e^{i\omega t}$ . It's also known as the TM field operator [34, 35], if  $\xi_i(t)$  meets the orthonormalization that  $\int dt \xi_i^*(t) \xi_j(t) = \delta_{ij}$ , for different  $i, j$ . The TM operators also obey the commutation relation, which reads

$$[\hat{A}_{\xi_i}, \hat{A}_{\xi_j}^\dagger] = \delta_{ij}. \quad (2)$$

It is then important to define the photon-wavepacket coherent state  $|\gamma_i\rangle_{\xi_i}$  on  $\xi_i$ -TM, as [33]

$$|\gamma_i\rangle_{\xi_i} = \hat{D}_{\xi_i}(\gamma_i)|0\rangle = \exp\left(\gamma_i \hat{A}_{\xi_i}^\dagger - \gamma_i^* \hat{A}_{\xi_i}\right)|0\rangle, \quad (3)$$

where  $\gamma_i$  denotes the displacement parameter,  $|\gamma_i|^2$  represents the average photon number. The photon-wavepacket coherent state obeys the eigenvalue equation,  $\hat{A}_{\xi_i}|\gamma_i\rangle_{\xi_i} = \gamma_i|\gamma_i\rangle_{\xi_i}$ . Under this notation, the quadrature operator with phase angle  $\theta$  can be defined as

$$\hat{X}_{\xi_i}^\theta = \hat{A}_{\xi_i}^\dagger \exp(i\theta) + \hat{A}_{\xi_i} \exp(-i\theta). \quad (4)$$

In a digital CVQKD system, coherent states are generated by widely-used in-phase/quadrature (I/Q) modulation. As shown in Fig. 1(a), assuming that  $|\gamma_0\rangle_{\xi_L}$  is the photon-wavepacket coherent state fed to the I/Q modulator,  $|\gamma_m\rangle_{\xi_L}$  are then the state of I or Q arm after the balanced beam splitter (BS), where  $\gamma_m = \gamma_0/\sqrt{2}$ . Then each arm performs the intensity modulation with certain waveform, which is modeled by a time-dependent BS with transmittivity  $\eta(t)$  related to modulation [38]. Assuming that the data encoded on the I and Q components in the  $i$ -th period are  $\{x_i\}$  and  $\{p_i\}$ , and their normalized waveform envelopes are  $\xi_I(t)$  and  $\xi_Q(t)$ , we can rewrite  $\sqrt{\eta_I(t)}\xi_L^0(t) = x_i\xi_I(t)$  on the I path and  $\sqrt{\eta_Q(t)}\xi_L^0(t) = p_i\xi_Q(t)$  on the Q path. Then the I and Q path's output states are transformed into  $|x_i\gamma_m\rangle_{\xi_I}$  and  $|p_i\gamma_m\rangle_{\xi_Q}$ . Finally, after passing through another balanced BS and a proper attenuator, the output photon-wavepacket coherent state is  $|x_i + ip_i\rangle_{\xi_{out}}$ , if  $\xi_I(t) = \xi_Q(t) = \xi_{out}(t)$  with properly calibrated modulation. This means in the entanglement-based scheme, the output coherent states can be seen as a two-mode squeezed states with  $\xi_{out}$ -TM being measured on one mode with heterodyne measurement. As for  $\xi_I(t) \neq \xi_Q(t)$ , the output state can be decomposed to two orthogonal TMs with different but correlated displacement parameters, which we leave for further investigations.

*Measurement, sampling and data processing.*—In the receiver side, the input state is first measured by a practical homodyne detector with limited bandwidth, then sampled by an analog-to-digital converter (ADC). After this, the sampled data go through a series of DSP algorithms, and the final data output from DSP is assumed to represent quadrature measurement result, which can be used to construct the covariance matrix and then calculate the secret key rate. We only consider linear DSP

algorithms here, since the transmitted quantum light is extremely weak that no obvious optical non-linear effects happen, thus linear compensation algorithms are enough to recovery the signal. By using the above continuous-mode formalism notation, mapping the outputs of linear DSP to quadrature measurements is surprisingly natural, in which the crucial step is normalization with properly calibrated SNU. To draw the core picture of this, we ignore the imperfections of homodyne detector and finite-resolution issue of ADC.

The receiver can be modeled as an ideal homodyne detector, followed by a filter, as shown in Fig. 1(b). Assuming the filter has an impulse response function (IRF), namely,  $g(t)$ , then the photocurrent flux operator of a homodyne detector is given by [33, 37]

$$\hat{f}(t) = [\hat{a}^\dagger(t) \hat{a}_{\text{LO}}(t) + \hat{a}_{\text{LO}}^\dagger(t) \hat{a}(t)] * g(t), \quad (5)$$

where  $*$  denotes the convolution. The photon wavepacket of the local oscillator (LO) is given by  $\alpha_{\text{LO}}(t) = \mu_{\text{LO}}^{1/2} \xi_{\text{LO}}(t) \exp(-i\omega_{\text{LO}}t + i\theta)$ , where  $\mu_{\text{LO}}$  denotes the average number of photons contained in an envelope  $\xi_{\text{LO}}(t)$  for a pulsed LO, or a time period as defined. Since LO is considered a classical field with enough many photons, the fluctuation of measurement output mainly comes from signal quadrature measurement part. Therefore, the photocurrent flux after taking average over LO is more useful, given by  $\hat{f}_{\text{LO}}(t) = \langle \alpha_{\text{LO}}(t) | \hat{f}(t) | \alpha_{\text{LO}}(t) \rangle$ .

Considering ADC as the integral sampling process with integral time  $\Delta t_s$ , the sampled data at time  $t_0$  is

$$\hat{D}_{t_0} = \frac{1}{\Delta t_s} \int_{t_0}^{t_0 + \Delta t_s} dt \hat{f}_{\text{LO}}(t), \quad (6)$$

in which the electronics amplification is ignored.

There may be multiple sampling points within one period  $T_r$ . Generally speaking, there are three types of linear data processing. i) Directly choose one sampled data of each period as final data of this period, for instance, the sampling point near the peak of the envelope of measured state. ii) Use sampled data within one period to define the final data of this period, for instance, calculating the weighted averaging of all sampled data within same period. iii) More generally, a DSP algorithm may use the sampled data from multiple periods, for instance, the Root Raised Cosine (RRC) filter [40] will introduce a convolution over multiple periods.

For a DSP algorithm involving  $N$  sampled data, the output data at the time corresponding to the  $t_j$  sampling time could be

$$\hat{D}_{t_j}^N = f_{\text{dsp}} \left( \hat{D}_{t_{j-k+1}}, \dots, \hat{D}_{t_{j-k+N}} \right) = \sum_{i=1}^N f_{\text{dsp}}^i \hat{D}_{t_{j-k+i}} \quad (7)$$

with linear expansion, where  $f_{\text{dsp}}^i$  and  $k$  are real numbers determined by DSP algorithms. After simplification, the

Eq. (7) is given by

$$\hat{D}_{t_j}^N = \frac{\mu_{\text{LO}}^{1/2}}{\Delta t_s} \int G_{\text{dsp}}^{t_j}(\tau) \hat{X}^{\alpha_{\text{LO}}}(\tau) d\tau, \quad (8)$$

where

$$G_{\text{dsp}}^{t_j}(\tau) = \sum_{i=1}^N f_{\text{dsp}}^i \int_{t_{j-k+i}}^{t_{j-k+i} + \Delta t_s} g(t - \tau) dt$$

is related to detector's IRF, sampling points and the DSP algorithm. And  $X^{\alpha_{\text{LO}}}(\tau)$  is the intermediate quadrature operator related to the LO's features, which is given by

$$\begin{aligned} \hat{X}^{\alpha_{\text{LO}}}(\tau) &= \xi_{\text{LO}}(\tau) e^{-i(\omega_{\text{LO}}\tau - \theta)} \hat{a}^\dagger(\tau) \\ &+ \xi_{\text{LO}}^*(\tau) e^{i(\omega_{\text{LO}}\tau - \theta)} \hat{a}(\tau). \end{aligned}$$

*SNU calibration and normalization.*—In order to normalize the output data from DSP, one key step is to define and calibrate the SNU, which is the most distinguishable phase from classical optical communication. Considering  $\hat{D}_{t_j}^N$  as the final data for the period where  $t_j$  lies in, then it's easy to verify for the vacuum input, the mean is  $\langle 0 | \hat{D}_{t_j}^N | 0 \rangle = 0$ , and the variance  $\sigma_{\text{SNU}}^2 = \langle 0 | \hat{D}_{t_j}^N \hat{D}_{t_j}^N | 0 \rangle$  is

$$\sigma_{\text{SNU}}^2 = \frac{\mu_{\text{LO}}}{\Delta t_s^2} \int |\xi_{\text{LO}}(\tau)|^2 \left[ G_{\text{dsp}}^{t_j}(\tau) \right]^2 d\tau. \quad (9)$$

For normalization, the sampled data  $\hat{D}_{t_j}^{\text{SNU}}$  is divided by  $\sigma_{\text{SNU}} = \sqrt{\sigma_{\text{SNU}}^2}$ , which gives

$$\hat{D}_{t_j}^{\text{SNU}} = e^{i\theta} \int d\tau \frac{G_{\text{dsp}}^{t_j}(\tau) \xi_{\text{LO}}(\tau) e^{-i\omega_{\text{LO}}\tau}}{\sigma_{\text{SNU}}} \hat{a}^\dagger(\tau) + \text{h.c.} \quad (10)$$

It can be verified that the coefficient function of  $\hat{a}(\tau)$  is a normalized photon-wavepacket function, which is

$$\Xi_{\text{DSP}}^{t_j}(\tau) = \frac{1}{\sigma_{\text{SNU}}} \xi_{\text{LO}}(\tau) G_{\text{dsp}}^{t_j}(\tau) \exp(-i\omega_{\text{LO}}\tau), \quad (11)$$

with normalization condition  $\int d\tau \left| \Xi_{\text{DSP}}^{t_j}(\tau) \right|^2 = 1$ . This introduces  $\Xi_{\text{DSP}}^{t_j}$ -TM, which is jointly defined by the LO, filter, sampling, and DSP algorithms. Then we can further define its creation operator as

$$\hat{A}_{\Xi_{\text{DSP}}^{t_j}}^\dagger = \int d\tau \Xi_{\text{DSP}}^{t_j}(\tau) \hat{a}^\dagger(\tau). \quad (12)$$

Consequently, a simplified form of Eq. (10) in terms of  $\Xi_{\text{DSP}}^{t_j}$ -TM operators is rewritten as

$$\hat{D}_{t_j}^{\text{SNU}} = \hat{A}_{\Xi_{\text{DSP}}^{t_j}}^\dagger \exp(i\theta) + \hat{A}_{\Xi_{\text{DSP}}^{t_j}} \exp(-i\theta) = \hat{X}_{\Xi_{\text{DSP}}^{t_j}}^\theta, \quad (13)$$

which shares the same form as Eq. (4).

Therefore, the final data (output from DSP and being normalized) can be treated as a quadrature measurement

of  $\Xi_{\text{DSP}}^{t_j}$ -TM. As long as it represents a quadrature measurement result, it can be used to construct the covariance matrix, thus compatible with traditional security analysis methods. The above analysis also points out one key guidance of SNU calibration, which is the sampled data of vacuum input should be processed by the same DSP as usual signal input case, before used to calculate the variance of shot noise.

Another important issue is, for a DSP involving sampled data exceeding one period, the possible crosstalk should be avoid. In this case, the TMs related to different periods should be orthogonal, i.e.,  $\int \Xi_{\text{DSP}}^{t_i} \Xi_{\text{DSP}}^{t_j*} = 0$ , where  $t_i, t_j$  belong to two different periods. This also coincides with classical DSP's purpose, as crosstalk will lower the SNR. For instance, the RRC pulse shaping and filtering are commonly used methods to improve the spectrum efficiency. In RRC filter, it is designed as no inter-symbol interference for different optimal sampling points, and this corresponds to the fact that the TMs related to different optimal sampling points are orthogonal.

This complete our security analysis framework for linear DSP, which can be summarized as two key points. One is properly calibrating SNU, which will naturally lead the final data to a quadrature measurement result, with respect to the TM defined jointly defined by LO, detector, sampling and DSP. The second is to avoid the complex measurement model introduced by intersymbol crosstalk, TMs corresponds to different periods should be orthogonal. If these two conditions apply, the final data can be directly used to construct the covariance matrix, and then calculate the secret key rate, as current security analysis method.

*Projection on measurement temporal mode.*—Beside security, our analysis also provides an understanding of imperfect detection efficiency, related to the mismatch between measured state's TM and the receiver's TM. The whole measurement process under the TM representation is equivalent to the projection of the measured state's TM to the receiver's TM, and vice versa.

Now consider a case where the measured state is a coherent state on  $\xi_A$ -TM, which is different to the receiver's  $\Xi_{\text{DSP}}^{t_j}$ -TM. Using the Gram-Schmidt orthogonalization, we can define a third TM from  $\Xi_{\text{DSP}}^{t_j}$ -TM and orthogonal to  $\xi_A$ -TM, denoted as  $\Psi_{\perp}$ -TM, which leads to the following decomposition of creation operator

$$\hat{A}_{\Xi_{\text{DSP}}^{t_j}}^{\dagger} = \sqrt{\eta} \hat{A}_{\xi_A}^{\dagger} + \sqrt{1-\eta} \hat{A}_{\Psi_{\perp}}^{\dagger},$$

where  $\eta = \left[ \Xi_{\text{DSP}}^{t_j*}(t) \xi_A(t) dt \right]^2 \leq 1$ . With further examination of the first-order and second-order moments, the above decomposition can be modeled by an extra BS at receiver side, with transmittivity  $\eta$ , quantifying the matching degree between  $\xi_A$ -TM and  $\Xi_{\text{DSP}}^{t_j}$ -TM.  $\eta < 1$  means an extra loss induced by the mode mismatch, which will decrease the performance of the system. This degradation is rather covert, different from the physical

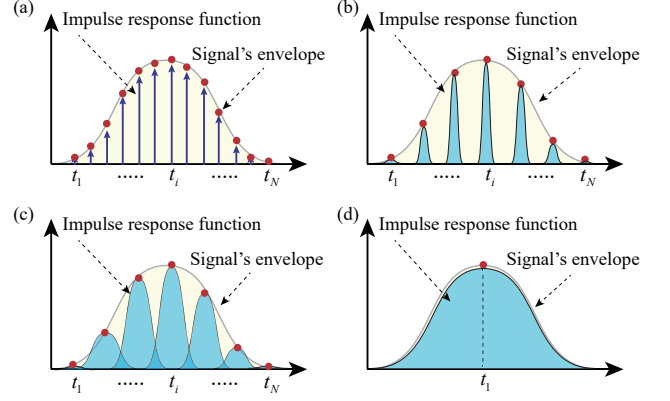


FIG. 2. Weighted averaging of sampled data. Assume the LO is a continuous-wave (CW) laser. (a) The bandwidth of the detector is large enough, and the impulse response function (IRF) is approximate to the  $\delta$ -function. The final data is recovered by weighted averaging of all sampled data within one period, and the weight follows the shape of the measured state's envelope. (b)(c) The bandwidth of detector is limited, resulting in a widened IRF, which convoluted the signal around each sampling point. (d) If the detector's IRF is similar to the measured state's envelope, single point sampling can represent the final data.

components introduced loss, i.e., fiber coupling loss, non-unit quantum efficiency of photodiodes. The closer of  $\eta$  to 1, the better performance a DSP algorithm is.

Here we take the weighted averaging scenario to further illustrate the mode matching issue in the time domain. In this case, the DSP function is given by  $f_{\text{dsp}}^i = w_i$ , where  $w_i$  is the weight of the  $i$ -th sampling point within one period. The measurement results can be described by Fig. 2. A sampled data does not only measure the signal at one time point, but also convoluted nearby signals around the sampling point. Therefore, an intuitive understanding of mode matching is that, the sum of all sampled data cover how much of the signal area. In Fig. 2(a), the bandwidth of the detector is large enough that the IRF is approximate to the  $\delta$ -function, then ultra-dense sampling is needed. While if the bandwidth becomes less and less, the IRF becomes wider and wider, less sampling points is required to achieve similar mode matching degree, as Fig. 2(b) (c). If the detector's IRF is similar to the measured state's envelope, single sampling point is enough, as in Fig. 2(d).

The measured state's TM is determined by the modulation at transmitter side, which is controlled, and also the channel transmission, which is not controlled. Therefore, the DSP need to be designed or adjusted according to the channel condition. We take channel dispersion as an example to show how it influence the measurement, which will become significant in a high-speed system. Considering a coherent state with narrow Gaussian wavepacket  $\xi_{\text{in}}(t)$ , after passing through the channel, its output envelope is transformed with a transfer function  $h(t, z)$ , given by  $\xi_{\text{out}}(t) = \xi_{\text{in}}(t) * h(t, z)$ , where



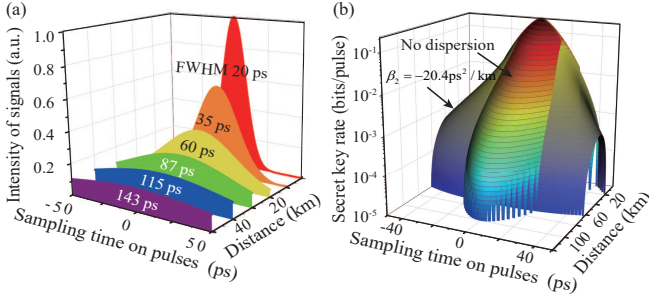


FIG. 3. Simulation results of channel dispersion effect. (a) Evolution of the envelope of a Gaussian pulse with a full width at half-maximum (FWHM) of 20 ps in optical fibers, ignoring the fiber loss. (b) Secret key rates for narrow-pulse (Gaussian pulse) propagation considering fiber dispersion induced TM mismatch, where no dispersion and  $\beta_2 = -20.4\text{ps}^2/\text{km}$  are considered. In the simulation, we use single sampling point scheme, and sampling time accuracy is considered. Sampling time  $t = 0\text{ps}$  is assumed as the peak of Gaussian pulse. It is shown that the increasing mode mismatch will reduce the secret key rate, while also relax the accuracy requirement of sampling time.

$h(t, z)$  is the channel transfer function in the time domain, and its Fourier transform is given by  $\mathcal{F}[h(t, z)] = \exp(-k_1 z + i k_1 \Omega z + i \frac{k_2}{2} \Omega^2 z)$ , in which the second-order Taylor expansion of the real part of the wave vector is considered,  $z$  is the transmission distance, and  $k_1$  and  $k_2$  denote the inverse group velocity and second-order dispersion coefficient, respectively. Only for ultrashort period, the influence of third-order nonlinear dispersion needs be considered. It can be seen the output state's TM varies with increasing distance as in Fig. 3(a). Therefore, if the DSP does not consider this TM varying, then there will be an increasing extra loss as transmission distance increases, which decreases the maximal transmission distance, as simulated in Fig. 3(b). This is where self-adaptive algorithms apply.

**Conclusions.**— In this study, we developed a generalized practical system model with continuous-mode formalism of quantum optics, based on which, the IQ modulation at transmitter side and band-limited homodyne detection with sampling process at receiver side can be well described. Then with proper calibration of SNU, the output data of a linear DSP can be seen as a quadrature measurement result, with respect to a specific TM, jointly defined by the LO, filter, sampling, and DSP algorithms. This immediately result in the compatibility with traditional security analysis methods, which completes the security proof of linear DSP algorithms. Linear DSP toolboxes are expected to be directly employed in CVQKD, which illustrates the importance of our work. Beside the security, our work also provides a method to analyze the performance of a DSP algorithm, through a factor quantifying the matching degree between the measured state's TM and the receiver's TM. In the meanwhile, interesting questions, like DSP induced fast fading-channel effect,

can be further analyzed to explore the practical limitations of a CVQKD system. By the guidance of our work, secure and better-performing DSP algorithms can be designed, which will release the significant potential of digital CVQKD to achieve ultra-high secret key generation speed and cost-effective implementations.

This work was supported by the National Natural Science Foundation of China (Grants Nos. 61531003 and 62001041), China Postdoctoral Science Foundation (Grant No. 2020TQ0016), and State Key Laboratory of Information Photonics and Optical Communications.

- 
- [1] N. Gisin, G. Ribordy, W. Tittel, H. Zbinden, Quantum cryptography, *Rev. Mod. Phys.* **74**, 145 (2002).
  - [2] S. Pirandola, U. L. Andersen, L. Banchi, M. Berta, D. Bunandar, R. Colbeck, D. Englund, T. Gehring, C. Lupo, C. Ottaviani, J. L. Pereira, M. Razavi, J. S. Shaari, M. Tomamichel, V. C. Usenko, G. Vallone, P. Villoresi, P. Wallden, Advances in quantum cryptography, *Adv. Opt. Photon.* **12**, 1012 (2020).
  - [3] F. Xu, X. Ma, Q. Zhang, H.-K. Lo, J.-W. Pan, Secure quantum key distribution with realistic devices, *Rev. Mod. Phys.* **92**, 025002 (2020).
  - [4] M. Peev *et al.*, The SECOQC quantum key distribution network in vienna, *New J. Phys.* **11**, 075001 (2009).
  - [5] M. Sasaki *et al.*, Tokyo QKD Network and the Evolution to Secure Photonic Network, in *CLEO: 2011 - Laser Science to Photonic Applications* (2011), pp. 1–3.
  - [6] Q. Zhang, F. Xu, Y.-A. Chen, C.-Z. Peng, J.-W. Pan, Large scale quantum key distribution: challenges and solutions, *Opt. Express* **26**, 24260 (2018).
  - [7] N. Hosseini-dehaj, Z. Babar, R. Malaney, S. X. Ng, L. Hanzo, Satellite-based continuous-variable quantum communications: State-of-the-art and a predictive outlook, *IEEE Communications Surveys Tutorials* **21**, 881 (2019).
  - [8] J. F. Dynes, A. Wonfor, W. W. S. Tam, A. W. Sharpe, R. Takahashi, M. Lucamarini, A. Plews, Z. L. Yuan, A. R. Dixon, J. Cho, Y. Tanizawa, J. P. Elbers, H. Greißer, I. H. White, R. V. Penty, A. J. Shields, Cambridge quantum network, *npj Quantum Inf.* **5**, 101 (2019).
  - [9] S. K. Joshi, D. Aktas, S. Wengerowsky, M. Lončarić, S. P. Neumann, B. Liu, T. Scheidl, G. C. Lorenzo, Ž. Samec, L. Kling, A. Qiu, M. Razavi, M. Stipčević, J. G. Rarity, R. Ursin, A trusted node-free eight-user metropolitan quantum communication network, *Sci. Adv.* **6**, eaba0959 (2020).
  - [10] T. K. Paraíso, T. Roger, D. G. Marangon, I. D. Marco, M. Sanzaro, R. I. Woodward, J. F. Dynes, Z. Yuan, A. J. Shields, A photonic integrated quantum secure communication system, *Nat. Photon.* **15**, 850 (2021).
  - [11] Y.-A. Chen *et al.*, An integrated space-to-ground quantum communication network over 4,600 kilometres, *Nature* **589**, 214 (2021).
  - [12] E. Diamanti, A. Leverrier, Distributing secret keys with quantum continuous variables: Principle, security and implementations, *Entropy* **17**, 6072 (2015).
  - [13] F. Laudenbach, C. Pacher, C.-H. F. Fung, A. Poppe, M. Peev, B. Schrenk, M. Hentschel, P. Walther, H. Hübel, Continuous-variable quantum key distribution with gaus-

- sian modulation—the theory of practical implementations, *Adv. Quantum Technol.* **1**, 1800011 (2018).
- [14] F. Grosshans, P. Grangier, Continuous variable quantum cryptography using coherent states, *Phys. Rev. Lett.* **88**, 057902 (2002).
  - [15] R. García-Patrón, N. J. Cerf, Unconditional optimality of Gaussian attacks against continuous-variable quantum key distribution, *Phys. Rev. Lett.* **97**, 190503 (2006).
  - [16] F. Furrer, T. Franz, M. Berta, A. Leverrier, V. B. Scholz, M. Tomamichel, R. F. Werner, Continuous variable quantum key distribution: Finite-key analysis of composable security against coherent attacks, *Phys. Rev. Lett.* **109**, 100502 (2012).
  - [17] A. Leverrier, Composable security proof for continuous variable quantum key distribution with coherent states, *Phys. Rev. Lett.* **114**, 070501 (2015).
  - [18] A. Leverrier, Security of continuous-variable quantum key distribution via a Gaussian de Finetti reduction, *Phys. Rev. Lett.* **118**, 200501 (2017).
  - [19] S. Pirandola, Limits and security of free-space quantum communications, *Phys. Rev. Research* **3**, 013279 (2021).
  - [20] S. Pirandola, Composable security for continuous variable quantum key distribution: Trust levels and practical key rates in wired and wireless networks, *Phys. Rev. Research* **3**, 043014 (2021).
  - [21] P. Jouguet, S. Kunz-Jacques, A. Leverrier, P. Grangier, E. Diamanti, Experimental demonstration of long-distance continuous-variable quantum key distribution, *Nat. Photon.* **7**, 378 (2013).
  - [22] D. Huang, P. Huang, D. Lin, G. Zeng, Long-distance continuous-variable quantum key distribution by controlling excess noise, *Sci. Rep.* **6**, 19201 (2016).
  - [23] Y. Zhang, Z. Chen, S. Pirandola, X. Wang, C. Zhou, B. Chu, Y. Zhao, B. Xu, S. Yu, H. Guo, Long-distance continuous-variable quantum key distribution over 202.81 km of fiber, *Phys. Rev. Lett.* **125**, 010502 (2020).
  - [24] B. Qi, P. Lougovski, R. Pooser, W. Grice, and M. Bobrek, Generating the Local Oscillator “Locally” in Continuous-Variable Quantum Key Distribution Based on Coherent Detection, *Phys. Rev. X* **5**, 041009 (2015).
  - [25] D. B. S. Soh, C. Brif, P. J. Coles, N. Lütkenhaus, R. M. Camacho, J. Urayama, and M. Sarovar, Self-Referenced Continuous-Variable Quantum Key Distribution Protocol, *Phys. Rev. X* **5**, 041010 (2015).
  - [26] F. Karinou, H. H. Brunner, C.-H. F. Fung, L. C. Comandar, S. Bettelli, D. Hillerkuss, M. Kuschnerov, S. Mikroulis, D. Wang, C. Xie, M. Peev, A. Poppe, Toward the integration of CV quantum key distribution in deployed optical networks, *IEEE Photon. Technol. Lett.* **30**, 650 (2018).
  - [27] T. A. Eriksson, T. Hirano, B. J. Puttnam, G. Rademacher, R. S. Luís, M. Fujiwara, R. Namiki, Y. Awaji, M. Takeoka, N. Wada, M. Sasaki, Wavelength division multiplexing of continuous variable quantum key distribution and 18.3 Tbit/s data channels, *Commun. Phys.* **2**, 9 (2019).
  - [28] T. A. Eriksson, R. S. Luís, B. J. Puttnam, G. Rademacher, M. Fujiwara, Y. Awaji, H. Furukawa, N. Wada, M. Takeoka, M. Sasaki, Wavelength division multiplexing of 194 continuous variable quantum key distribution channels, *J. Lightwave Technol.* **38**, 2214 (2020).
  - [29] H. Wang et al., Sub-Gbps Key Rate Four-State Continuous-Variable Quantum Key Distribution within Metropolitan Area, *Commun Phys* **5**, 162 (2022).
  - [30] Z. Li, Y.-C. Zhang, H. Guo, User-defined quantum key distribution, *arXiv:1805.04249* (2018).
  - [31] S. Ghorai, P. Grangier, E. Diamanti, and A. Leverrier, Asymptotic Security of Continuous-Variable Quantum Key Distribution with a Discrete Modulation, *Phys. Rev. X* **9**, 021059 (2019).
  - [32] J. Lin, T. Upadhyaya, and N. Lütkenhaus, Asymptotic Security Analysis of Discrete-Modulated Continuous-Variable Quantum Key Distribution, *Phys. Rev. X* **9**, 041064 (2019).
  - [33] K. J. Blow, R. Loudon, S. J. D. Phoenix, T. J. Shepherd, Continuum fields in quantum optics, *Phys. Rev. A* **42**, 4102 (1990).
  - [34] C. Fabre and N. Treps, Modes and States in Quantum Optics, *Rev. Mod. Phys.* **92**, 40 (2020).
  - [35] M. G. Raymer and I. A. Walmsley, Temporal Modes in Quantum Optics: Then and Now, *Phys. Scr.* **95**, 064002 (2020).
  - [36] M. G. Raymer, Z. W. Li, and I. A. Walmsley, Temporal Quantum Fluctuations in Stimulated Raman Scattering: Coherent-Modes Description, *Phys. Rev. Lett.* **63**, 1586 (1989).
  - [37] R. Loudon, *The Quantum Theory of Light: 3rd Edition* (Oxford University Press, New York, 2000).
  - [38] H.-A. Bachor and T. C. Ralph, *A Guide to Experiments in Quantum Optics: 3rd Edition* (Wiley-VCH, Berlin, 2019).
  - [39] M. J. Collett, R. Loudon, and C. W. Gardiner, Quantum Theory of Optical Homodyne and Heterodyne Detection, *J. Mod. Opt.* **34**, 881 (1987).
  - [40] N. S. Alagha, and P. Kabal, Generalized raised-cosine filters. *IEEE transactions on Communications*, **47**, 989 (1999).